Plasmon excitation in single-walled carbon nanotubes probed using charged particles: comparison of calculated and experimental spectra

2013 J. Phys.: Condens. Matter 25 175001

(http://iopscience.iop.org/0953-8984/25/17/175001)

IOP PUBLISHING JOURNAL OF PHYSICS: CONDENSED MATTER

J. Phys.: Condens. Matter **25** (2013) 175001 (9pp) doi:10.1088/0953-8984/25/17/175001

Plasmon excitation in single-walled carbon nanotubes probed using charged particles: comparison of calculated and experimental spectra

Silvina Segui[1,2], **Zoran L Mišković**[3], **Juana L Gervasoni**[1,2,4] **and Néstor R Arista**[1,4]

[1] Centro Atómico Bariloche, Comisión Nacional de Energía Atómica, Avenida Bustillo 9500, 8400 San Carlos de Bariloche, Argentina
[2] Consejo Nacional de Investigaciones Científicas y Técnicas, Argentina
[3] Department of Applied Mathematics, and the Waterloo Institute for Nanotechnology, University of Waterloo, Waterloo, ON, N2L 3G1, Canada
[4] Instituto Balseiro (Universidad Nacional de Cuyo and Comisión Nacional de Energía Atómica), Avenida Bustillo 9500, 8400 San Carlos de Bariloche, Argentina

E-mail: segui@cab.cnea.gov.ar

Received 21 November 2012
Published 18 March 2013
Online at stacks.iop.org/JPhysCM/25/175001

Abstract
We study ‘ the excitation of plasmons due to the incidence of a fast charged particle that passes through a single-wall carbon nanotube. We use a quantized hydrodynamic model, in which the σ and π electron systems are depicted as two interacting fluids moving on a cylindrical surface. Calculations of the average number of the excited plasmons and the corresponding energy loss probability for the swift electrons are compared with several experimental results for electron energy loss spectra recorded using transmission electron microscopes. We are able to identify the π and $\sigma + \pi$ plasmon peaks and elucidate the origin of various spectral features observed in different experiments.

(Some figures may appear in colour only in the online journal)

1. Introduction

The study of plasmon excitations in carbon nanotubes is of prime interest for a variety of applications, e.g. in the context of their optical response. These excitations are efficiently probed by using charged particles, as in the electron energy loss spectroscopy (EELS) technique performed with a transmission electron microscope (TEM). There is a considerable body of literature, both theoretical [1–9] and experimental [10–15], dedicated to the study of plasmon excitations in single-walled and multi-walled carbon nanotubes, both isolated and assembled in bundles or other configurations. However, there are some observations that remain unexplained or have not been completely elucidated. For example, the exact role of surface plasmons in spectral features observed for losses at high energy remains unclear [13].

Considering the geometry of single-walled carbon nanotubes (SWCNTs) and the characteristics of their electronic structure, the excitation of plasmons is conveniently described by a two-fluid formulation of the hydrodynamic model [6]. In this formulation, σ and π electrons are treated as two-dimensional (2D) fluids constrained to the same cylindrical surface. The electrostatic interaction between the fluids gives rise to splitting of their plasmon frequencies into two groups of distinct energies, usually referred to as ‘$\sigma + \pi$’ (high energy) and ‘π’ (low energy) plasmons. Moreover, a quantized version of the hydrodynamic model [8] enables one to calculate the average number of plasmons excited in different modes by a fast charged particle impinging on an

SWCNT. This formulation also provides a relatively simple way to evaluate the energy loss probability density that may be directly compared with the spectra recorded in various EELS experiments on SWCNTs.

In [8] we used the quantized hydrodynamic model to perform qualitative analysis of the spectra of plasmon excitations in SWCNTs due to fast electrons moving along the trajectories that are external to the nanotubes. It should be noted that those spectra are characterized by narrow spectral features due to the neglect of plasmon damping, which is inherent to the quantization approach. In this work we make several extensions of this model that allow us to make quantitative comparison with several experimental spectra [11–13] where characteristic plasmon peaks exhibit substantial broadening. Besides the inclusion of electron trajectories that traverse the nanotube with an arbitrary impact point, we thoroughly analyze the parameters involved in the formulation of the hydrodynamic model in order to determine their values for which calculations reproduce the principal features of the experimental spectra. In particular, we include the effect of plasmon damping that amounts to broadening of the theoretical spectra and we reconsider the role of plasmon restoring frequencies that reflect the band structure effects for the σ and π electrons.

The paper is structured as follows. In section 2 we briefly comment on the parameterization of the hydrodynamical model used to describe the excitation of plasmon modes in SWCNTs. In section 3 we summarize the basic formulas used for calculation of the average number of plasmons excited by an incident charged particle and its energy loss probability density. In section 4 we compare the calculated energy loss spectra with experimental data from the literature and analyze their main features. Finally, we state our concluding remarks in section 5.

2. Plasmon modes within the hydrodynamic model

We use the quantized 2D two-fluid hydrodynamical model for describing the excitation of plasmons in carbon nanotubes, which was presented in [8]. In that paper, we applied a quantization procedure [16] to the semiclassical hydrodynamic model [6] to describe the excitation of plasmons[5] by charged particles within an interaction-picture framework where the Coulomb potential from the external electron excites various modes in the plasmon field. This formulation allows us to obtain the energy lost by the incident particle in terms of the average number of plasmon modes excited.

The hydrodynamical model provides an analytical expression for the dispersion relation, $\omega_{\pm,m,k}$, for plasmon modes that appear on a cylindrical surface containing the interacting σ and π electrons fluids, defined by

$$\omega_{\pm,m,k}^2 = \frac{\omega_\sigma^2 + \omega_\pi^2}{2} \pm \sqrt{\left(\frac{\omega_\sigma^2 - \omega_\pi^2}{2}\right)^2 + \Delta^4}. \qquad (1)$$

[5] In the SWCNT geometry and within the 2D hydrodynamic model, the only collective excitations are surface plasmons.

Here, ω_ν are the plasmon frequencies of the non-interacting $\nu = \sigma$ and $\nu = \pi$ fluids, and Δ accounts for the interaction between them. These quantities are defined by the geometry of the system and depend on the usual angular modes $m = 0, \pm 1, \pm 2, \ldots$, and the longitudinal wavenumber k. The coupling of the two fluids yields two branches of modes: the high energy modes (obtained with the '+' sign in equation (1)) are the so-called '$\sigma + \pi$' modes, which exhibit wide dispersion as a function of both k and m, whereas the low energy modes (obtained with the '−' sign), or π plasmons, exhibit less dispersion.

One of the features of the model proposed for describing the dispersion $\omega_{\pm,m,k}$ is the inclusion of restoring frequencies $\omega_{\nu,r}$, which take into account the band structure of the valence electrons that constitute each fluid. For instance, σ electrons are known to have a semiconductor/dielectric band structure with a band gap of about ≈10 eV. That is, σ electrons need to absorb a minimum amount of energy $\hbar\omega_{\sigma,r}$ larger than ≈10 eV to participate in any collective oscillation. On the other hand, π electrons have a semimetal (with zero gap) or semiconductor (with a band gap of ≈2 eV) structure, depending on the geometry and chirality of the nanotube. Hence, $\hbar\omega_{\pi,r}$ may take a value from zero to a few electronvolts. In our previous work [8], we took as a first approximation the values $\omega_{\pi,r} = 0$ and $\hbar\omega_{\sigma,r} = 16$ eV, following the work of Barton and Eberlein [17] and Gorokhov *et al* [18] who suggested these values for the π and σ electrons of a C_{60} molecule. We note that using these values for restoring frequencies in equation (1) gives a dispersion relation that accurately describes the available experimental results [10, 14, 15], as shown in [8].

On the other hand, recent studies on graphene [19] showed that a finite value for the restoring frequency of the π electrons (around 4 eV) and a lower value for the σ electrons (around 13 eV) are suitable for describing the energy loss spectra in monolayered and multilayered graphene. In the present work we adopt the set of values obtained for graphene in [19], $\hbar\omega_{\sigma,r} = 13.08$ eV and $\hbar\omega_{\pi,r} = 4.06$ eV, as these values seem to be *a priori* in better agreement with the positions of plasmon peaks observed in the experiments on SWCNTs [11–13]. We note that using these values for restoring frequencies in equation (1) gives a dispersion relation, shown in figure 1(a), that also exhibits quite good agreement with the experimental results [10, 14, 15]. One of the most interesting features of plasmons in nanoscopic systems is the sensitivity of their characteristic frequencies to variations in the geometry. Figure 1(b) illustrates the dispersion relation (1) for the first two modes ($m = 0$ and $m = 1$) and for both branches (π and $\sigma + \pi$) for different values of the nanotube's radius R. As one can see, the frequencies allowed in the $m = 0$ mode do not vary significantly with R, but the $m = 1$ (and higher) modes are very sensitive to its variation, especially in the region with low k, which gives the principal contribution to the plasmon excitation spectra.

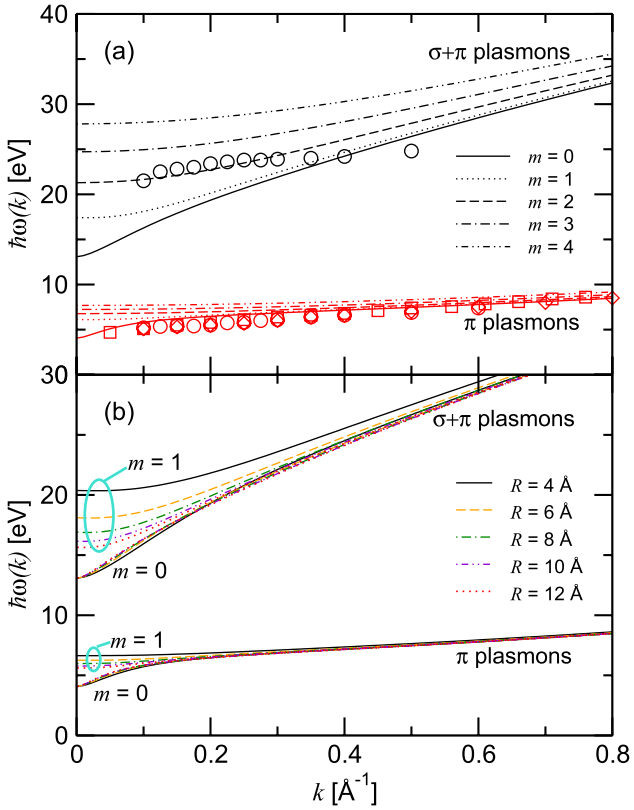

Figure 1. Dispersion relation ω_{jmk} as a function of k, using the graphene values for the restoring frequencies $\omega_{\pi,r} = 4.06$ eV and $\omega_{\sigma,r} = 13.08$ eV. (a) Modes $m = 0, 1, \ldots, 4$ are compared with the experimental dispersions from Pichler *et al* [10] (circles) and Kramberger *et al* [14, 15] (diamonds and squares) for a nanotube with $R = 7$ Å. (b) Dispersion of the modes $m = 0$ and $m = 1$ for several nanotube radii R.

3. Excitation of plasmons and the energy loss probability

The quantization procedure applied to the hydrodynamical model allows us to evaluate the average number of plasmons μ_{jmk} excited in a mode $\{j, m, k\}$, where j stands for $\pm$, on an SWCNT of radius R by an incident electron following an arbitrary trajectory as follows [8]:

$$\mu_{jmk} = C_{jmk}\,|\check{V}_{\rm ext}(R; m, k, \omega_{jmk})|^2. \tag{2}$$

The factor C_{jmk} contains information regarding the available modes of the plasmon field, and is obtained as

$$C_{jmk} = \frac{n_0}{\mathcal{A}}\,\frac{D^2_{jmk}}{2m_*}\,\frac{\frac{m^2}{R^2} + k^2}{\omega_{jmk}}, \tag{3}$$

where n_0 and m_* are the total number density and the mean effective mass of the σ and π fluids, respectively, $\mathcal{A}$ is the area of the cylindrical surface occupied by the fluids, and D_{jmk} is a function which takes values in the interval $[-1, 1]$ and depends on plasmon frequencies of the non-interacting fluids and on the coupling between them (see [8] for details). The interaction with the incident electron is included through $\check{V}_{\rm ext}(R; m, k, \omega)$, which is a Fourier–Bessel transform of the Coulomb potential created by a point charge e moving on a general trajectory, given by $\mathbf{r}_0(t) = (r_0(t), \phi_0(t), z(t))$ in cylindrical coordinates. We have

$$\check{V}_{\rm ext}(R; m, k, \omega) = \int_{-\infty}^{\infty} {\rm d}t\, {\rm e}^{{\rm i}\omega t}\widetilde{V}_{\rm ext}(R; m, k, t), \tag{4}$$

where

$$\widetilde{V}_{\rm ext}(R; m, k, t) = -e^2 Z R\, g_{mk}(R, r_0(t))\, {\rm e}^{-{\rm i}m\phi_0(t) - {\rm i}kz_0(t)} \tag{5}$$

with $g_{mk}(r, r') = 4\pi I_{\rm m}(|k|r_<)K_{\rm m}(|k|r_>)$ being the cylindrical Green function, in which $r_< = {\rm Min}(r, r')$ and $r_> = {\rm Max}(r, r')$, whereas $I_{\rm m}$ and $K_{\rm m}$ are the modified Bessel functions of the first and second kind, respectively.

In this work we are interested in comparing our results with the energy loss spectra obtained with a TEM using the EELS technique, with the electron beam typically accelerated at ≈100 keV or more. Since the total energy losses due to plasmon excitation are small (namely, less than 50 eV), we may consider that the electrons follow straight-line trajectories without deflection. Moreover, we restrict our calculations to the trajectories that are perpendicular to the nanotube's axis, which is the most usual experimental setting. Hence, we may write the coordinates of the incident electron as

$$\begin{aligned} r_0(t) &= \sqrt{r^2_{\rm min} + (vt)^2}, \\ \phi_0(t) &= \arctan\left(\frac{vt}{r_{\rm min}}\right), \\ z_0(t) &= 0, \end{aligned} \tag{6}$$

where $r_{\rm min}$ is the minimum distance to the tube's axis (or impact parameter).

While the integral in equation (4) may be evaluated analytically for external trajectories with $r_{\rm min} \geq R$, as shown in [8], in the case of trajectories traversing the nanotube we obtain from (4)

$$\begin{aligned} \check{V}_{\rm ext}(R; m, k, \omega_{jmk}) = -8\pi e^2 R[&K_{\rm m}(|k|R) f^{\pm}_{jmk} \\ &+ I_{\rm m}(|k|R)\, h^{\pm}_{jmk}], \end{aligned} \tag{7}$$

where

$$f^{\pm}_{jmk} = \int_0^{t_0} {\rm d}t\, I_{\rm m}(|k|\sqrt{r^2_{\rm min} + (vt)^2})\, \cos(\omega_{jmk}t - m\phi_0(t)), \tag{8}$$

$$\begin{aligned} h^{\pm}_{jmk} = &\int_{t_0}^{\infty} {\rm d}t\, K_{\rm m}(|k|\sqrt{r^2_{\rm min} + (vt)^2}) \\ &\times \cos(\omega_{jmk}t - m\phi_0(t)), \end{aligned} \tag{9}$$

with $t_0 = \sqrt{R^2 - r^2_{\rm min}}/v$ defining the instants $\pm t_0$ at which the electron crosses the nanotube wall. Thus, the average number of plasmons excited in a given mode, μ_{jmk}, is given by

$$\mu_{jmk} = (8\pi)^2 e^4 R^2 C_{jmk} |K_{\rm m}(|k|R) f^{\pm}_{jmk} + I_{\rm m}(|k|R)\, h^{\pm}_{jmk}|^2. \tag{10}$$

Since we consider only the perpendicular trajectories, μ_{jmk} is an even function of k. In the case where the electron crosses the nanotube through its axis, μ_{jmk} is also an even

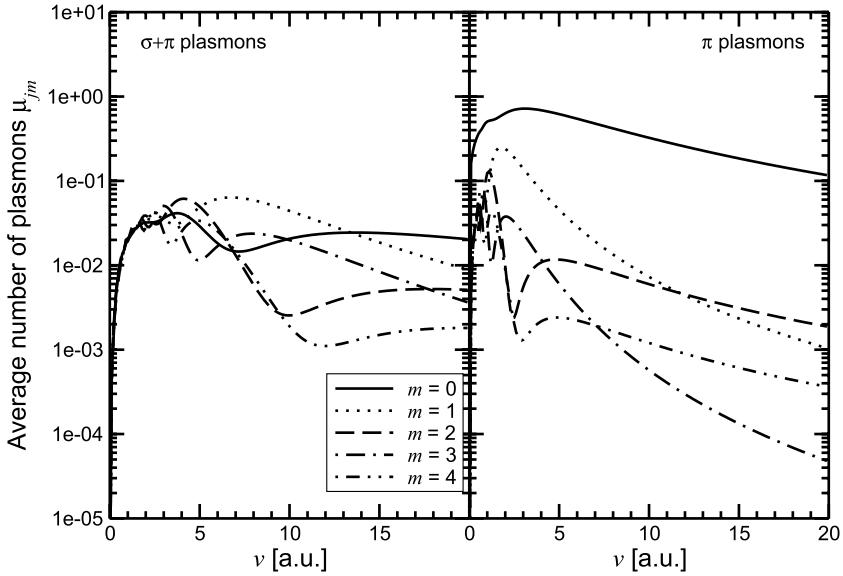

Figure 2. Average number of plasmons μ_{jm}, integrated over k, for an SWCNT of radius $R = 7$ Å, excited by an electron passing through the nanotube's axis ($r_{\min} = 0$).

function of m. In the latter case, the angle $\phi_0(t)$ is defined as

$$\phi_0(t) = \begin{cases} -\dfrac{\pi}{2}, & t < 0, \\ +\dfrac{\pi}{2}, & t \geq 0. \end{cases}$$

In figure 2 we plot the integrated average number of plasmons excited in the mode $\{j, m\}$, $\mu_{jm} = \int_{-\infty}^{\infty} \mu_{jmk}\, \mathrm{d}k$, as a function of the incident electron speed v for a trajectory passing through the axis of a 7 Å radius nanotube. It is interesting to compare the complex behavior of different modes with those observed in [8] for external trajectories. In the present case, there are multiple oscillations in which the predominance of even and odd modes alternates with varying speed. The period of these oscillations tends to increase at larger values of the impact parameter $r_{\min}$, until they completely disappear when the trajectory becomes entirely external to the nanotube. Similar oscillations were also observed in cylindrical wires [20] and even in planar surfaces [21], suggesting that under certain conditions on the projectile speed and nanotube radius some modes may be virtually suppressed.

With the above definition of the average number of plasmons excited by an energetic electron following a straight-line trajectory through or near a nanotube, we may obtain the probability density for such an electron losing a given amount of energy ε as

$$\begin{aligned} P(\varepsilon) &= \sum_{jmk} \mu_{jmk} \delta(\varepsilon - \hbar\omega_{jmk}) \\ &= \sum_m \frac{L}{2\pi} \int_{-\infty}^{\infty} \mathrm{d}k \sum_{j=\pm} C_{jmk} \delta(\varepsilon - \hbar\omega_{jmk}) \\ &\quad \times |\check{V}_{\mathrm{ext}}(R; m, k, \varepsilon/\hbar)|^2. \end{aligned} \tag{11}$$

We note that $P(\varepsilon)$ is proportional to the intensity of spectra recorded in the EELS experiments.

Notice that the δ-function in (11) selects, for each $\{j, m\}$ mode, a value of k for which the allowed energy $\hbar\omega_{jmk}$ equals the energy loss ε considered. This gives rise to spectra with narrow but asymmetric peaks, since the dispersion relation in figure 1 shows that ω_{jmk} increases monotonically with k. In order to facilitate comparison with experimental spectra, where narrow peaks are broadened due to intrinsic plasmon damping, as well as due to extrinsic experimental factors, we calculate $P(\varepsilon)$ by introducing an empirical damping rate γ. Accordingly, we substitute the delta function $\delta(\varepsilon - \hbar\omega_{jmk})$ in equation (11) by the Lorentzian of the form [22]

$$\delta(\varepsilon - \hbar\omega_{jmk}) \longrightarrow \frac{\gamma/\pi}{(\varepsilon - \hbar\omega_{jmk})^2 + \gamma^2}. \tag{12}$$

We note that this kind of broadening of the plasmon spectra naturally arises in the semiclassical version of the hydrodynamic model where the effects of damping are taken into account at the outset in the formulation of the model [8]. However, a precise value of γ is not well defined and, moreover, γ could take different values for each of the fluids. However, we consider, as a first approximation, the same value of γ for both the σ and π electron fluids, and take $\hbar\gamma = 3$ eV in close agreement with the value adopted in a recent application of the hydrodynamic model to graphene [19].

4. Energy loss spectra: results and discussion

In this section we show and analyze the energy loss spectra, calculated using the formalism of the previous section. Many basic features of the energy loss process due to plasmon excitation are more clearly seen in the undamped spectra calculated with $\gamma = 0$. Hence, we first analyze the characteristics of $P(\varepsilon)$ calculated from equation (11) with different geometrical parameters $r_{\min}$ and R, and then we proceed to include finite damping to compare with the experimental spectra found in the literature.

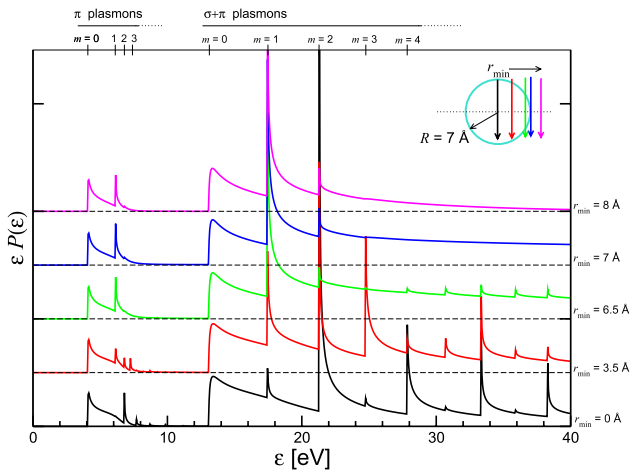

Figure 3. Calculated spectra with different values of $r_{\min}$, the minimum distance from the particle's trajectory to the axis of a nanotube of radius $R = 7$ Å for incident electrons with energy $E_0 = 100$ keV. Ticks in the upper axis indicate the values of $\omega_{\pm,m,0}$ for each mode.

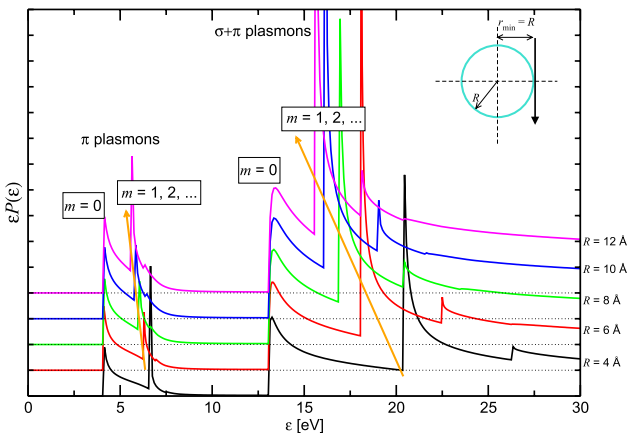

Figure 4. Calculated spectra with different values of the nanotube's radius R, for incident electrons with energy $E_0 = 100$ keV, on the trajectories passing at $r_{\min} = R$.

In figure 3 we plot the dimensionless product $\varepsilon P(\varepsilon)$ to facilitate discussion of the energy loss probability with zero damping for a 100 keV electron passing perpendicularly through a 7 Å nanotube at different impact parameters $r_{\min}$. The upper scale in this figure indicates the energy values corresponding to the different m modes at $k = 0$ according to figure 1, which serves to identify the m values corresponding to each peak in the energy spectra. We note that the contributions of higher m modes ($m > 2$) are almost completely suppressed for external trajectories, but are enhanced for penetrating trajectories, reaching maximum values when the electron passes through the nanotube center. Moreover, relative contributions of different modes change when $r_{\min}$ varies between the nanotube center and the nanotube wall. For instance, considering the $\sigma + \pi$ modes at $r_{\min} = 0$, contributions from the odd modes ($m = 1, 3, 5, \ldots$) are heavily suppressed with respect to the neighboring even modes, whereas the $m = 1$ (or the dipole) mode dominates the spectrum for external trajectories. This behavior of various m modes is related to the oscillations observed in the average number of plasmons, shown in figure 2.

Also of interest is the variation of spectrum when the nanotube radius R changes. We plot in figure 4, in correspondence with the dispersion relations shown in figure 1, the calculated spectra for electron trajectories that are tangential to the walls of nanotubes of various radii. Again considering the $\sigma + \pi$ modes, one notices that the positions of the asymmetric peaks corresponding to the $m = 0$ mode remain unaffected by the change in R, whereas the positions of the peaks due to the $m = 1, 2, \ldots$ modes move to lower energies with increasing R. This behavior of spectral contributions of various modes is in accord with the behavior of the dispersion relations shown in figure 1(b). It is worth mentioning that one can show that the positions of the sharp jumps on the left hand sides of all the $m = 0$ peaks in figure 4 are determined by the restoring frequency of the σ electrons, $\hbar\omega_{\sigma,r} \approx 13$ eV, whereas the distance of the jumps in the $m = 1$ peaks from $\hbar\omega_{\sigma,r}$ (i.e., their energy differences) are approximately given by $\hbar\pi e^2 n_\sigma/(R\omega_{\sigma,r}) \approx 30\,R^{-1}$ eV Å, where $n_\sigma \approx 114.7$ nm^{-2} is the equilibrium surface density of σ electrons.

4.1. Comparison with experimental spectra

We have selected, among the various experimental works [10–15] reporting on the energy loss spectra of carbon nanotubes in different configurations and geometries, those by Reed and Sarikaya [11], Stöckli *et al* [12], and Stéphan *et al* [13] because they correspond to isolated SWCNTs and the spectra were taken under similar conditions. Figures 5–7 show the results of our calculations of $P(\varepsilon)$, in units of eV^{-1}, while the experimental data are renormalized (with different factors) to be commensurate with the theoretical values.

Reed and Sarikaya recorded several spectra corresponding to SWCNTs, both in isolated and in bundled samples. In particular, a free-standing nanotube with a 12 Å diameter was studied with two different positions of the electron beam: traversing the nanotube and passing remotely. The authors fitted their spectra using a sum of Lorentzian functions in order to obtain the energy losses corresponding to the excitation of plasmons and some intra-band transitions.

Stöckli *et al* reported spectra obtained from an $R = 6.1$ Å SWCNT and an $R = 6.7$ Å SWCNT, which were supposedly crossed by the incident beam through their axes. The spectra showed peaks around the energy losses corresponding to the $\sigma + \pi$ plasmon. However, no peak was observed for the plasmon of low energy, probably because it was hidden by the zero-loss peak. In that work, the authors also compared their results with the spectra calculated from a semiclassical hydrodynamical model, for which they considered a single fluid with the plasma parameters taken from the bulk graphite data.

Stéphan *et al* studied single-walled and multi-walled carbon nanotubes of different sizes and recorded the energy loss spectra for 100 keV electrons at grazing trajectories (i.e., with the impact parameter equal to the radius of each

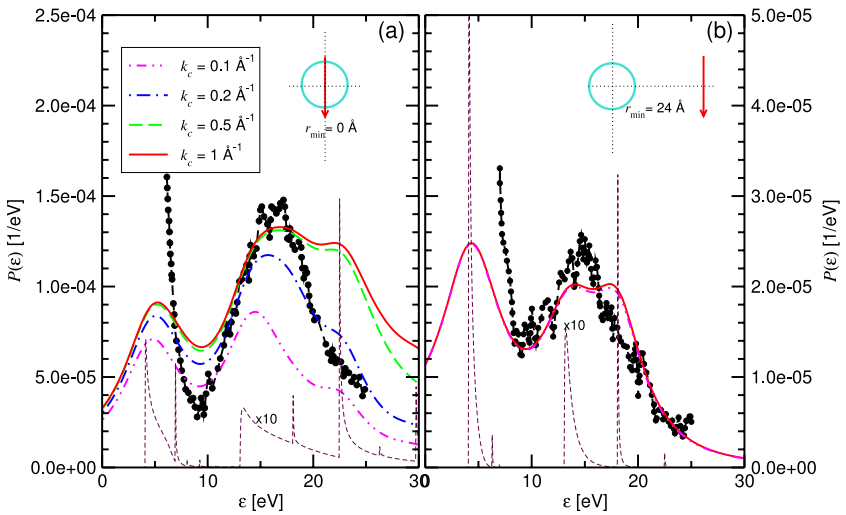

Figure 5. Comparison of calculated spectra with experimental spectra reported by Reed and Sarikaya [11], corresponding to an SWCNT of 6 Å radius and two impact parameters: (a) $r_{\min} = 0$ and (b) $r_{\min} = 24$ Å . Thin dashed line: energy loss probability distribution $P(\varepsilon)$ in units of eV^{-1} with zero damping ($\gamma = 0$). Smooth colored lines: probability distribution with finite damping ($\gamma = 3$ eV) for various values of the momentum transfer cutoff k_c. Dashed line with circles: experimental data. The remaining parameters are: beam energy $E_0 = 100$ keV, and restoring frequencies $\omega_{\pi r} = 4.06$ eV, $\omega_{\sigma r} = 13.08$ eV.

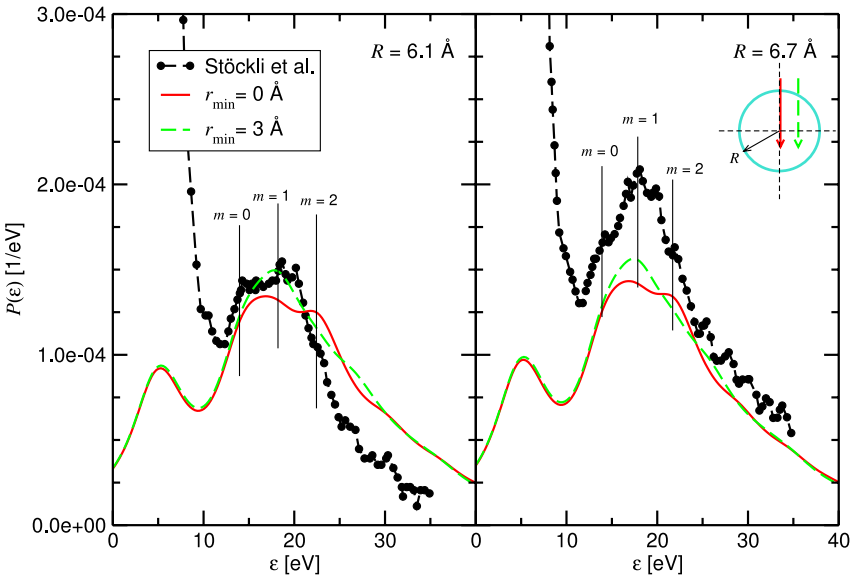

Figure 6. Comparison of calculated spectra with experimental spectra reported by Stöckli *et al* [12] (black dashed line with circles) for SWCNTs of radii $R = 6.1$ Å and $R = 6.7$ Å, with the electron beam impinging perpendicularly at the nanotubes. Two impact parameters are considered, $r_{\min} = 0$ (red line) and $r_{\min} = 3$ Å (green line). The remaining parameters are: beam energy $E_0 = 100$ keV, restoring frequencies $\omega_{\pi r} = 4.06$ eV, $\omega_{\sigma r} = 13.08$ eV, and the momentum transfer cutoff $k_c = 1$ Å^{-1}.

nanotube). In particular, they recorded the spectra for a 6 Å SWCNT and an 11 Å SWCNT, and compared their results with calculations based on a semiclassical dielectric model for the bulk dielectric function of graphite.

In principle, the above experimental studies detected peaks at characteristic energy losses that may be identified with the π and $\sigma + \pi$ plasmons. The peak at low energy, when visible, is easily distinguished around 5 eV, which may be explained by a confluence of the multiple peaks with $m = 0, 1, 2, \ldots$, seen in the idealized spectra of figures 3 and 4, which is caused by the intrinsic plasmon damping and the low dispersion of the π modes seen in figure 1. On the other hand, more variability and more structure is observed in experiments for the high energy, $\sigma + \pi$ plasmon modes. There is a general agreement among the authors that there are at least two features, labeled I and II, occurring at a lower energy of ≈14–15 eV and a higher energy of ≈19 eV, respectively. Those features are tentatively ascribed to surface plasmon excitations, depending on the size of the nanotubes considered [13]. Table 1 gives a synthesis of the characteristic energies observed by different authors.

We have calculated the energy loss probability density for comparison with the experimental spectra by considering in each case the radii and the impact parameters as reported by

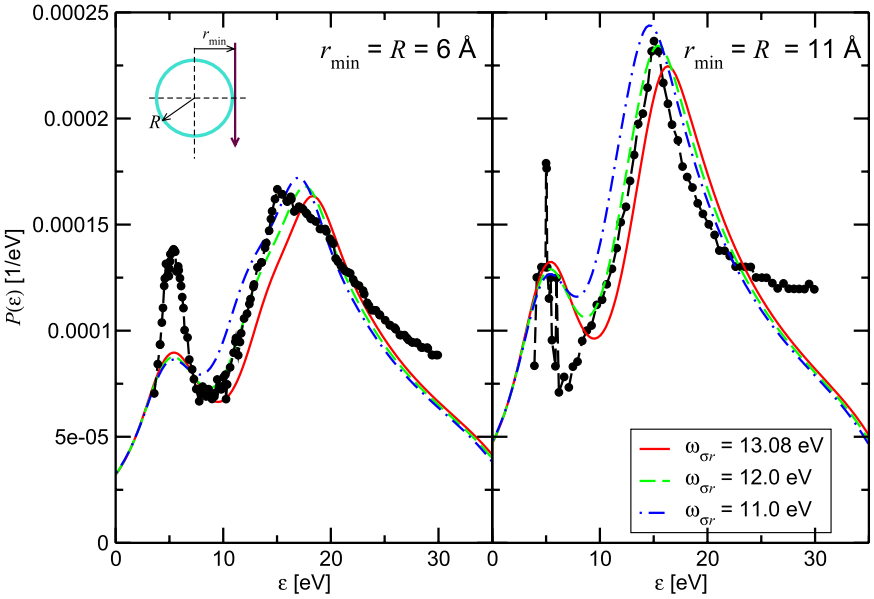

Figure 7. Comparison of calculated spectra with experimental spectra reported by Stéphan *et al* [13], for nanotubes with the radii 6 Å (left panel) and 11 Å (right panel) and the beam passing at tangential trajectories ($r_{\min} = R$). We used a fixed restoring frequency of $\omega_{\pi,r} = 4.06$ eV for π electrons, and varying restoring frequency for σ electrons: $\omega_{\sigma,r} = 13.08$ eV (red continuous line), 12 eV (green dashed line) and 11 eV (blue dash–dotted line). Black dashed line with circles: experimental data.

Table 1. Comparison of the $\sigma + \pi$ plasmon energies identified by different authors in their EELS experiments. I and II identify the lower and higher peak/shoulder observed.

Reference	R (Å)		Energy (eV)
Reed and Sarikaya [11]	6	I	13–15
		II	17–19
Stöckli *et al* [12]	6.1	I	14
		II	19.5
	6.7	I	13.5
		II	19
Stéphan *et al* [13]	6	I	15
		II	19
	11	I	15
		II	—

the authors of the cited works. In these calculations we have adopted a damping parameter that has the same value of $\hbar\gamma = 3$ eV for both fluids. In addition, we have introduced a cutoff in the longitudinal momentum transfer, k_c, in the integral of equation (11), above which single-particle excitations start to dominate over the collective excitations. This restriction influences the shape of the spectra by suppressing higher energy peaks observed in figure 3 that correspond to the modes excited with larger momentum transfers. A reasonable value for this parameter is $k_c \sim 1$ Å^{-1}.

In figure 5 we compare the calculated spectra with the measurements by Reed and Sarikaya, obtained with the beam passing through the axis of a 6 Å radius nanotube and at a distance of about 24 Å from it. We display the results of calculations with different values of k_c in order to show the variability of the theoretical spectrum, especially for penetrating trajectories. Also included is the corresponding zero-damping spectrum calculated with no momentum cutoff, which is useful for identifying the contributions of different m modes. The penetrating trajectory calculations (with $r_{\min} = 0$) show great variability with k_c, especially in view of the rapid suppression of the $m = 2$ mode at low k_c values. The figure shows that the broad peak centered at ≈16.5 eV in the spectra recorded by Reed and Sarikaya may be attributed to the contribution of the broad $m = 0$ feature and the much less prominent $m = 1$ mode, while the small shoulder at ≈22 eV corresponds to the excitation of the $m = 2$ mode. The relative contribution of the modes is not satisfactorily reproduced by the theoretical spectrum at $k_c = 1$ Å^{-1}. In that respect we observe that, although the position of the electron beam reported by the authors is $r_{\min} = 0$, it is possible that the finite size of the beam spot influences the results, with some electron trajectories passing at a considerable distance from the nanotube axis and contributing to the spectrum with different weights of the $m > 0$ modes, as shown in figure 3.

The issue of the observed suppression of the higher m modes in comparison with theoretical spectra may also be tackled by postulating a cutoff value in the angular momentum, m_c, beyond which collective oscillations around the nanotube circumference dissipate into single-particle excitations. For example, Barton and Eberlein [17] found a cutoff of $\ell_c = 3$ for the spherical angular plasmon modes on a C_{60} molecule. Further comments on the weights coming form different m modes in the losses at high energy are given below, in our analysis of the spectra measured by Stöckli *et al*.

Regarding the external trajectory, we observe that the calculated spectra are less sensitive to the value of k_c (hence only the results with $k_c = 0.1$ and 1 Å^{-1} are shown). Clearly, the peak of the experimental spectrum corresponds to the $m = 0$ contribution, while the $m = 1$ contribution at ≈17.5 eV is less visible in the experimental spectrum. (Also, notice that

the probability density at this large value of $r_{\min}$ is about 5 times smaller than the corresponding values at penetrating trajectories.)

We further present in figure 6 a comparison with the data recorded by Stöckli *et al*, corresponding to two SWNTs of similar radii, $R = 6.1$ Å (figure 6(a)) and $R = 6.7$ Å (figure 6(b)). The raw spectra measured by these authors are very noisy, and were treated with a high frequency filter to facilitate the identification of certain features between ≈14 eV and ≈22 eV for both nanotubes. One may infer from the paper by Stöckli *et al* that the electron beam, which traverses the nanotubes perpendicularly and is centered on their axes, covers more than a half of each nanotube's diameter, assuming the spot size of about 5 Å. Hence, it is reasonable to consider that the electrons of the beam cross the nanotube with impact parameters in a range from $r_{\min} = 0$ to $r_{\min} \approx 2.5$–3 Å. Taking this into account, we have included in figure 6 the results of calculations for trajectories with $r_{\min} = 0$ (thick red lines) and trajectories with $r_{\min} = 3$ Å (thick green lines). As one can see, while the position of different contributions from the modes $m = 0, 1, 2, \ldots$ may be associated with features observed in the experimental spectra, the general shape and the relative contribution of these modes are better reproduced by the off-center trajectories in both nanotubes.

It should be mentioned that Stöckli *et al* have also compared their data with their own calculations based on a hydrodynamic model, and analyzed the spectra on the basis of their numerical results. In particular, since they considered only the excitation of $\sigma + \pi$ plasmons and did not include any restoring terms, the dispersion relation for their $m = 0$ mode vanishes in the $k \to 0$ limit, in contrast with what we obtain by using finite restoring frequencies. This fact makes their $m = 0$ contribution negligible above energy losses of about 10 eV, while our approach yields a large contribution from that mode right above the threshold given by $\hbar\omega_{\sigma,r}$. As a consequence, they identify the peak at ≈14 eV in the experimental spectra with the $m = 1$ mode, while we postulate that the broad feature seen between 14 and 19 eV is largely due to a mixture of contributions from the $m = 0$ and 1 modes. A sharp test for proving our assertion is based on the experimental observation that the position of the feature at ≈14 eV practically does not vary with the nanotube radius, while the position of the feature below ≈20 eV associated with the $m = 1$ mode is shifted to a somewhat higher energy in the thinner nanotube. While this argument is qualitatively supported by the discussion of theoretical spectra in figure 4, the energy resolution of the experimental data is not sufficient for full quantitative validation.

Finally, in figure 7 we analyze the data recorded by Stéphan *et al* [13]. These spectra were taken also at 100 keV, with an electron probe having a 0.5 nm diameter, and with electron trajectories being perpendicular to the nanotubes and presumably tangential to their walls. The spectra include a loss region at low energy, with a clearly identifiable contribution of the π plasmon at around 5.1 eV. This peak is relatively well reproduced by our model and it does not undergo much change in going from the 6 Å nanotube to the 11 Å nanotube, in accordance with the spectra in figure 4. Regarding the losses at high energy, the experimental data present a marked peak at around 15 eV, which is broader for the thinner nanotube. At this energy, as seen in figure 3, the dominant modes are $m = 0$ and 1, so we may assert that the distance between them (i.e., the difference of the energies of these modes) governs the width of the peak that is shown in the calculated spectra. We recall from figure 4 that the distance between these modes decreases with increasing nanotube radius, while the position of the $m = 0$ contribution remains unchanged.

We also include in figure 7 calculations made with different values of the restoring frequency $\omega_{\sigma,r}$, in order to show the dependence of the position of the $\sigma + \pi$ plasmon peak on this parameter. It can be seen that the plasmon peak energy is very sensitive to $\omega_{\sigma,r}$ and it shifts by an amount on the same order as the variation in the restoring frequency. Since the value of this empirical parameter is related to, but not unequivocally determined by, the energy gap, $\omega_{\sigma,r}$ may vary with the dimension and chirality of the nanotube considered.

5. Conclusions

We have implemented a calculation of the energy loss spectra due to plasmon excitation for fast electrons passing through a single-walled carbon nanotube, thereby extending the methodology of a quantized two-dimensional, two-fluid hydrodynamic model developed in a previous work for remote external trajectories [8]. This methodology allows calculation of the average number of excited plasmons and the corresponding probability density of the energy loss with zero damping, which provide valuable information on the role of various plasmon modes in the spectra and their dependence on geometric factors such as the electron beam impact parameter and the nanotube radius. We have further compared our results with the experimental spectra recorded by three different groups using electron energy loss spectroscopy with a transmission electron microscope. In an attempt to elucidate the origins of different features in those spectra, we have included a finite value for the plasmon damping rate, introduced a maximum momentum transfer for incident electrons, and modified the values of the restoring frequencies for the σ and π electron systems in accord with recent implementation of the hydrodynamic model for graphene.

The π plasmon peak, located around 5 eV, is easily identified and well reproduced by the calculations, in consistency with the very good performance shown by the present model in describing the corresponding dispersion relation [8]. The relatively compact structure of the π plasmon peak and its stability against change in the nanotube radius are explained by a confluence of the contributions due to different angular modes of order $m = 0, 1, 2, \ldots$, which exhibit weak dispersion.

On the other hand, the high energy $\sigma + \pi$ plasmon peak shows more structure in both the experimental spectra and our calculations, presumably because of the broader dispersion of its angular modes and a more pronounced sensitivity to the nanotube radius than in the case of the π plasmon. We were

able to obtain a reasonable qualitative agreement between the calculations and the experimental spectra and, in particular, we identified structures around 13 and 19 eV in those spectra as being attributable to the angular modes with $m = 0$ and 1 of the $\sigma + \pi$ plasmon.

Hence, we may conclude that the inclusion of restoring frequencies in the hydrodynamic model, combined with different weights of the principal angular modes that depend on geometric factors, yields an explanation of the loss features at high energy in the spectra, without the need to invoke bulk properties of graphite for single-walled carbon nanotubes [13]. However, quantitative details of the experimental spectra are difficult to reproduce because the calculated spectra are found to be very sensitive to different parameters of the model. In particular, the finite size of the incident electron beam spot seems to greatly affect the calculated spectra for trajectories passing through the nanotube, and we shall tackle this aspect of the model in future work.

Acknowledgments

We thank for fruitful discussions MS Moreno, who helped us to understand the experimental issues. We gratefully acknowledge partial financial support from CONICET (PIP112 20090100670) and Universidad Nacional de Cuyo. ZLM acknowledges support from the Natural Sciences and Engineering Research Council of Canada.

References

[1] Lin M F and Shung K W K 1993 Elementary excitations in cylindrical tubules *Phys. Rev.* B **47** 6617–24
[2] Sato O, Kobayashi M, Tanaka Y and Hasegawa A 1995 Acoustic plasma wave in a quantum-size cylindrical electron–hole plasma *Phys. Rev.* B **52** 4677–9
[3] Yannouleas C, Bogachek E N and Landman U 1996 Collective excitations of multishell carbon microstructures: multishell fullerenes and coaxial nanotubes *Phys. Rev.* B **53** 10225–36
[4] Stöckli T, Wang Z L, Bonard J-M, Stadelmann P and Châtelain A 1999 Plasmon excitations in carbon nanotubes *Phil. Mag.* B **79** 1531–48
[5] Taverna D, Kociak M, Charbois V and Henrard L 2002 Electron energy-loss spectrum of an electron passing near a locally anisotropic nanotube *Phys. Rev.* B **66** 235419
[6] Mowbray D J, Mišković Z L, Goodman F O and Wang Y-N 2004 Interactions of fast ions with carbon nanotubes: two-fluid model *Phys. Rev.* B **70** 195418
[7] Gumbs G and Balassis A 2005 Comparison of the stopping power of plasmons and single-particle excitations for nanotubes *Phys. Rev.* B **71** 235410
[8] Mowbray D J, Segui S, Gervasoni J, Mišković Z L and Arista N R 2010 Plasmon excitations on a single-wall carbon nanotube by external charges: two-dimensional two-fluid hydrodynamic model *Phys. Rev.* B **82** 035405
[9] Kyriakou I, Emfietzoglou D, García-Molina R, Abril I and Kostarelos K 2011 Simple model of bulk and surface excitation effects to inelastic scattering in low-energy electron beam irradiation of multi-walled carbon nanotubes *J. Appl. Phys.* **110** 054304
[10] Pichler T, Knupfer M, Golden M S, Fink J, Rinzler A and Smalley R E 1998 Localized and delocalized electronic states in single-wall carbon nanotubes *Phys. Rev. Lett.* **80** 4729–32
[11] Reed B W and Sarikaya M 2001 Electronic properties of carbon nanotubes by transmission electron energy-loss spectroscopy *Phys. Rev.* B **64** 195404
[12] Stöckli T, Bonard J-M, Châtelain A, Wang Z L and Stadelmann P 2002 Valence excitations in individual single-wall carbon nanotubes *Appl. Phys. Lett.* **80** 2982
[13] Stéphan O, Taverna D, Kociak M, Suenaga K, Henrard L and Colliex C 2002 Dielectric response of isolated carbon nanotubes investigated by spatially resolved electron energy-loss spectroscopy: from multiwalled to single-walled nanotubes *Phys. Rev.* B **66** 155422
[14] Kramberger C, Hambach R, Giorgetti C, Rümmeli M H, Knupfer M, Fink J, Büchner B, Reining L, Einarsson E, Maruyama S, Sottile F, Hannewald K, Olevano V, Marinopoulos A G and Pichler T 2008 Linear plasmon dispersion in single-wall carbon nanotubes and the collective excitation spectrum of graphene *Phys. Rev. Lett.* **100** 196803
[15] Kramberger C, Rümmeli M, Knupfer M, Fink J, Büchner B, Einarsson E, Maruyama S and Pichler T 2008 *Phys. Status Solidi* b **245** 2284
[16] Arista N R and Fuentes M A 2001 Interaction of charged particles with surface plasmons in cylindrical channels in solids *Phys. Rev.* B **63** 165401
[17] Barton G and Eberlein C 1991 Plasma spectroscopy proposed for C_{60} and C_{70} *J. Chem. Phys.* **95** 1512
[18] Gorokhov D A, Suris R A and Cheianov V V 1996 Electron-energy-loss spectroscopy of the C60 molecule *Phys. Lett.* A **223** 116
[19] Borka Jovanović V, Radović I, Borka D and Mišković Z L 2011 High-energy plasmon spectroscopy of freestanding multilayer graphene *Phys. Rev.* B **84** 155416
[20] Gervasoni J L and Arista N R 2003 Plasmon excitations in cylindrical wires by external charged particles *Phys. Rev.* B **68** 235302
[21] Denton C, Gervasoni J L, Barrachina R O and Arista N R 1998 Plasmon excitation by charged particles moving near a solid surface *Phys. Rev.* A **57** 4498–511
[22] Lucas A A, Benedek G, Sunjic M and Echenique P M 2011 Theory of highly charged ion energy gain spectroscopy of molecular collective excitations *New J. Phys.* **13** 013034